metals

MDPI

Article

Thermodynamic and Pilot-Scale Experimental Analysis of Medium-Carbon Ferromanganese Production

Assylbek Abdirashit, Bakyt Suleimen *, Bagdagul Uakhitova, Rustem Uakhitov *, Meruert Taizhigitova and Amanbek Nurtayev

Department of Metallurgy and Mining, K. Zhubanov Aktobe Regional University, Aktobe 030000, Kazakhstan; aabdirashit@zhubanov.edu.kz (A.A.); buakhitova@zhubanov.edu.kz (B.U.); mtaizhigitova@zhubanov.edu.kz (M.T.); technical@zhubanov.edu.kz (A.N.)

* Correspondence: b.suleimen@zhubanov.edu.kz (B.S.); ruakhitov@zhubanov.edu.kz (R.U.); Tel.: +7-777-434-2758 (B.S.)

Abstract

This study investigates the thermodynamic and technological aspects of smelting medium-carbon ferromanganese from Zhezdinsky manganese ore using ferrosilicomanganese and lime. The equilibrium distribution of components in the oxide-metal system was calculated using HSC Chemistry 10.0 within the temperature range of 573–2073 K. The modeling results revealed the effect of lime and ore consumption on slag phase composition as well as on manganese and silicon contents in the metallic phase. Experimental validation was performed in a laboratory Tamman resistance furnace and in a 100 kVA large-scale laboratory electric arc furnace. The chemical compositions of metal and slag were determined by bulk chemical analysis, while microstructure and local elemental distribution were examined using SEM-EDS. An increase in slag basicity was found to promote the transfer of silicon into the silicate phase while simultaneously reducing manganese losses to the slag. The large-scale laboratory smelting experiments, with a duration of 100–120 min per heat, enabled the establishment of a stable processing regime and the production of a metal with an average composition of 88.1 wt.% Mn, 1.6 wt.% C, and 0.03 wt.% Si. The corresponding slag contained approximately 15 wt.% MnO and 21 wt.% SiO_2. SEM-EDS analysis showed that the alloy possesses a heterogeneous microstructure consisting of an Fe-Mn metallic matrix with finely dispersed silicide microphases. Local silicon concentrations in these phases reach 15–24 wt.%, which explains the discrepancy between local and bulk chemical compositions. The experimental data are in good quantitative agreement with the thermodynamic modeling results, confirming that slag basicity and composition control are key factors for improving manganese recovery and stabilizing metal composition. The identified relationships can be applied in the development of industrially oriented smelting regimes for producing medium-carbon ferromanganese from Kazakhstan manganese raw materials.

Keywords: medium-carbon ferromanganese; manganese ore; lime; thermodynamic modeling; HSC Chemistry; 100 kVA electric arc furnace; SEM-EDS; slag; basicity

Check for updates

Academic Editor: Dmitri Molodov

Received: 3 February 2026
Revised: 19 February 2026
Accepted: 20 February 2026
Published: 22 February 2026

Copyright: © 2026 by the authors. Licensee MDPI, Basel, Switzerland. This article is an open access article distributed under the terms and conditions of the Creative Commons Attribution (CC BY) license.

1. Introduction

Manganese is one of the key alloying and deoxidizing elements in ferrous metallurgy. Manganese-containing ferroalloys—primarily ferromanganese and silicomanganese—are widely used in the production of pig iron and steel, providing deoxidation, desulfurization,

and control of metal structure [1,2]. Medium-carbon ferromanganese (MCFeMn) is particularly in demand for the production of high-quality and special steels, where limited carbon and impurity contents are required. The quality of ferromanganese directly affects steel cleanliness, since nonmetallic inclusions formed during alloy production can transfer into the steel melt [1].

The production of manganese ferroalloys is governed by complex thermodynamic and kinetic interactions between metallic, slag, and gas phases. One of the key process objectives is the reduction of manganese oxides and the minimization of MnO losses to the slag. It has been established that the reduction degree of MnO strongly depends on slag basicity, temperature, and carbon activity in the system [3,4]. Thermodynamic analyses of carbon behavior in liquid manganese and ferromanganese melts confirm that carbon solubility and activity significantly influence phase equilibria and reduction reactions during smelting [5].

Industrial production of refined manganese ferroalloys is based on carbothermic and silicothermic processes, depending on the required carbon content in the final product. Silicothermic reduction is widely used for the production of medium- and low-carbon ferromanganese, as it enables a reduction in carbon content while maintaining a high manganese recovery [2,6]. The choice of reductant (typically carbonaceous materials such as coke, coal, or charcoal in conventional processes or silicon from ferrosilicomanganese in metallothermic routes) and slag-forming additives plays a decisive role in controlling metal composition and minimizing manganese losses to the slag [7–9].

Modern developments in ferromanganese production technology are also associated with the processing of low-grade manganese ores and secondary raw materials. The possibility of producing ferromanganese from low-grade ores using alternative reductants, including charcoal and biomass, has been demonstrated, particularly in small-scale and pilot electric arc furnaces [10]. The pre-reduction of manganese ores prior to smelting improves manganese recovery and reduces energy consumption [11]. Recent thermodynamic and experimental studies also confirm the effectiveness of combined reduction systems and controlled slag formation in the processing of technogenic and low-grade manganese materials [12–14].

Despite the substantial body of research devoted to high-carbon ferromanganese, the thermodynamics and technology of medium-carbon ferromanganese production under conditions close to industrial practice have been studied to a lesser extent. In particular, the influence of slag composition and technological parameters on element distribution between metallic and slag phases remains a relevant issue. This requires an integrated approach combining thermodynamic modeling and experimental validation in enlarged laboratory-scale units, which allows optimization of the MCFeMn smelting process, increased manganese recovery, and controlled silicon and carbon contents in the alloy [6,7].

The global refined ferromanganese market is characterized by a high concentration of production. According to data from the International Manganese Institute and the USGS, the main producers are China, Norway, the Republic of Korea, and India, which account for the majority of global refined manganese alloy output [15,16]. At the same time, recent years have seen fluctuations in production due to changes in steel demand and imbalances between manganese ore mining and manganese consumption in metallurgy.

Kazakhstan possesses significant manganese ore reserves and ranks among the leading countries in their extraction [16,17]. However, a substantial portion of these ores is characterized by elevated contents of silica, phosphorus, and iron, which complicates their direct use in metallurgical processes [18,19]. The absence of a universal integrated technology for processing ores of varying composition limits the efficient utilization of domestic raw materials in manganese ferroalloy production [18–20].

Scientific research on the processing of Kazakhstan manganese ores is actively conducted at the Zh. Abishev Chemical-Metallurgical Institute and other research centers [21–25]. Approaches involving the use of highly basic slags, combined reductants, and thermodynamically justified smelting regimes are being developed [26]. However, industrial production of medium-carbon ferromanganese in Kazakhstan is practically absent, leading to dependence on imports of this product, primarily from major producing countries such as China, India, and Russia, despite the availability of a domestic raw material base.

Thus, the development of a scientifically grounded technology for smelting medium-carbon ferromanganese from Kazakhstan manganese raw materials is an urgent task aimed at increasing the depth of mineral resource processing, reducing import dependence, and improving the efficiency of the national metallurgical sector.

2. Materials and Methods

2.1. Raw Materials

In the study of the smelting process of medium-carbon ferromanganese, Zhezdinsky manganese ore, ferrosilicomanganese, and lime were used as raw materials. The chemical compositions of the materials are presented in Table 1, and the appearance of the initial materials is shown in Figure 1.

Table 1. Chemical Composition of the Initial Charge Materials, wt.%.

Materials	$Mn_{general}$	SiO_2	Al_2O_3	Fe_2O_3	MgO	CaO	P_2O_5	S
Manganese ore	47–48	12.48	2.76	3.45	1.47	1.28	0.03	0.01
Lime	-	1	0.18	0.62	1.14	90	0.005	0.005
SiMn 17	Mn		Si		Fe	S	P	C
	60–65		16–18		7–10	0.05	0.05	1.0–2.5

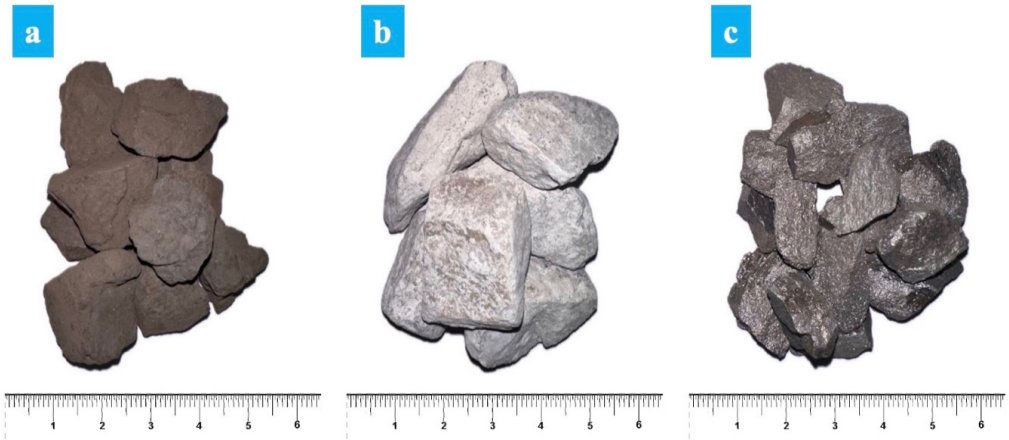


Figure 1. General view of the charge materials: (**a**) manganese ore, (**b**) lime, (**c**) FeSiMn 17.

2.2. Thermodynamic Modeling

Thermodynamic modeling of the medium-carbon ferromanganese smelting process was carried out using the HSC Chemistry 10.0 software package [27,28]. This package contains an extensive thermochemical database, including data on enthalpy (H), entropy (S), and heat capacity (C) for more than 29,000 chemical compounds. HSC Chemistry 10.0 includes more than ten calculation modules. In the present study, the Equilibrium Compositions module was used, which is based on the calculation of the equilibrium composition of a system according to the Gibbs free energy minimization principle [29,30].

The equilibrium composition of the multicomponent "oxide-metal" system was determined using the Equilibrium Compositions module over the temperature range of 573–2073 K with a step of 100 K, assuming a constant gas-phase pressure equal to 1 atm.

In the thermodynamic modeling, the amount of ferrosilicomanganese was fixed at 100 kg, while the consumption of manganese ore and lime was varied. This approach was adopted because ferrosilicomanganese acts as a stable silicon-bearing reductant and a source of metallic components in the system. Maintaining its constant amount makes it possible to isolate and quantitatively assess the influence of slag-forming additions and oxide raw materials on phase equilibria.

Variation of manganese ore consumption changes the input of manganese and gangue oxides into the system, thereby affecting the redox balance, slag composition, and the distribution of manganese between metal and slag. Adjustment of lime addition directly controls slag basicity (CaO/SiO_2 ratio), which is one of the key thermodynamic parameters governing the activity of oxide components, the stability of silicate phases, and the recovery of manganese.

Thus, fixing the ferrosilicomanganese input while varying ore and lime consumption provides a controlled framework for evaluating how slag chemistry and oxide loading influence reduction reactions and the final composition of the metallic phase, particularly the contents of manganese, silicon, iron, and carbon. This approach allows the determination of optimal slag basicity and charge proportions required to obtain medium-carbon ferromanganese with target Mn and Si contents.

2.3. Experimental Smelting

Experimental studies on the smelting of medium-carbon ferromanganese were carried out in a laboratory high-temperature Tamman-type resistance furnace. This furnace is designed for simulating metallurgical processes under laboratory conditions. The working zone of the unit is constructed as a graphite tube, and temperature control was achieved using a thyristor voltage regulator. Since the thyristor regulator is connected to the primary winding of the power transformer, the output busbars provide currents of several thousand amperes at reduced voltages (0.5–15 V). The furnace temperature was measured using a tungsten–rhenium thermocouple (VR-5/20) placed in a corundum protective sheath [31,32].

In addition, large-scale laboratory smelting experiments of medium-carbon ferromanganese were performed in a 100 kVA electric arc furnace, allowing the evaluation of process behavior under conditions close to industrial practice [33,34].

Preheating of the electric arc furnace was conducted for approximately 8 h using coke breeze. After completion of the heating stage, the coke powder was removed and the main charge materials were loaded into the furnace. The operating transformer voltage was 49 V.

The refining furnace was lined with MP-95-grade magnesite refractory bricks, and the joints between the bricks were filled with magnesite powder. The furnace was equipped with two graphitized electrodes with a diameter of 100 mm. A cross-sectional view of the electric arc furnace is shown in Figure 2.

Figure 2 shows a cross-sectional view of the 100 kVA electric arc furnace with transformer used for the experimental smelting trials. Heating and melting of the charge are achieved by an electric arc formed between the graphite electrodes (1) and the melt. The electrodes are secured in electrode holders (2), which provide their fixation and allow vertical position adjustment during the smelting process.

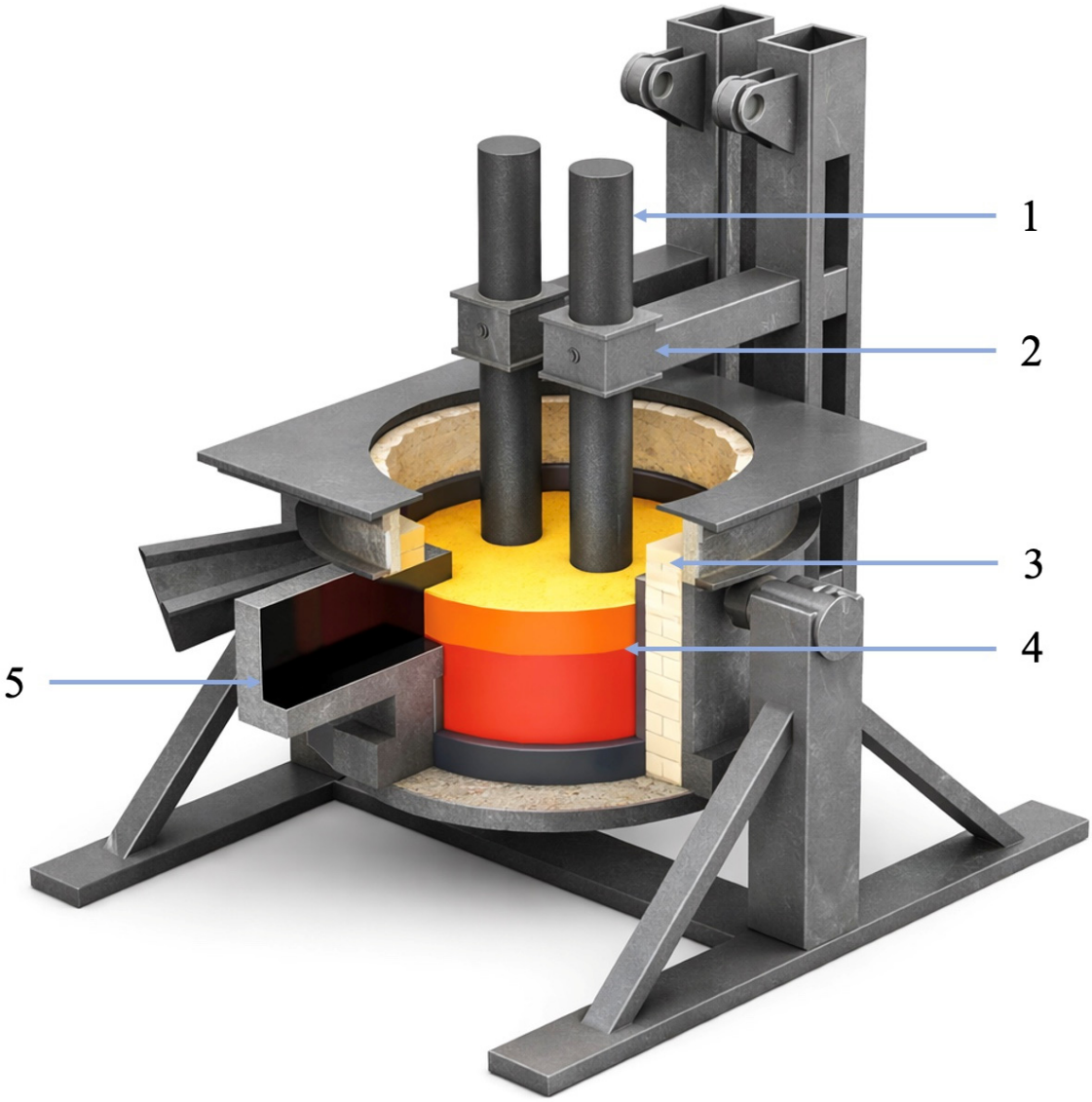


Figure 2. Cross-sectional view of the 100 kVA electric arc furnace with transformer. 1—graphite electrode; 2—electrode holder; 3—lining (magnesite brick); 4—melt (metal and slag); 5—tap hole.

The inner surface of the furnace is lined with magnesite refractory bricks (3), ensuring high thermal resistance and chemical stability of the lining in contact with basic slags. Within the working space of the furnace, a melt (4) is formed, consisting of metallic and slag phases, where the main reduction and refining processes take place. Tapping of the finished metal and slag is carried out through the tap hole (5) located in the lower part of the furnace. The presented design ensures a stable thermal regime and efficient progression of metallurgical processes under large-scale laboratory conditions.

2.4. Microstructural Investigation by SEM

The microstructure of the medium-carbon ferromanganese sample was investigated using scanning electron microscopy (SEM) with a JEOL JXA-8230 (JEOL Ltd., Tokyo, Japan) instrument, followed by energy-dispersive spectroscopy (EDS) for the analysis of individual microstructural constituents. The microscope enables imaging in both secondary electron (SE) and backscattered electron (BSE) modes, allowing detailed characterization of surface morphology as well as compositional contrast between phases with different average atomic numbers.

SEM examinations were carried out under high-vacuum conditions at an accelerating voltage in the range of 15–20 kV. Local chemical characterization included point analyses, line scans, and elemental mapping to determine the spatial distribution of the principal elements within the alloy. The obtained analytical results were processed using standard matrix correction procedures to improve the accuracy and reliability of the quantitative data.

3. Results and Discussion

3.1. Thermodynamic Calculation

3.1.1. Thermodynamic Modeling of Lime Consumption During Medium-Carbon Ferromanganese Smelting

The consumption of manganese ore and lime adopted for the thermodynamic modeling, calculated per 100 kg of ferrosilicomanganese, is presented in Table 2.

Table 2. Consumption of Charge Materials, kg.

FeSiMn 17	Manganese Ore	Lime
100	100	0–145

Lime consumption was varied in the range of 0–145 kg with a step of 10 kg. Figure 3 shows the dependence of calcium-containing compounds in the slag phase on temperature and the amount of added lime (CaO). The thermodynamic modeling results illustrate the distribution of the main calcium-bearing phases, including free CaO and calcium silicates of various compositions.

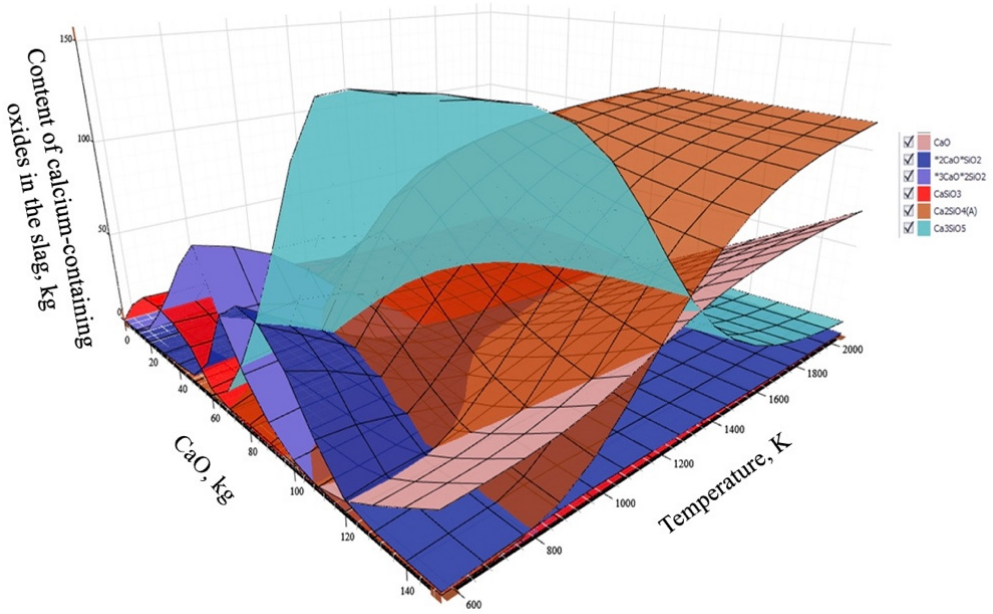


Figure 3. Dependence of the Content of Calcium-Containing Oxide Compounds in Slag on Temperature and Lime Consumption.

The variation in slag phase composition as a function of lime consumption and temperature was analyzed by thermodynamic modeling in the temperature range of 573–2073 K. It was established that the formation of calcium silicates begins at relatively low temperatures.

In the range of 573–873 K, calcium silicate $CaSiO_3$ is formed. At lime additions of 30–120 kg within the same temperature interval, dicalcium silicate $2CaO{\cdot}SiO_2$ (Ca_2SiO_4) forms in amounts ranging from 0 to 57.6 kg. With an increase in temperature to 800–2073 K,

the content of dicalcium silicate increases further, reaching 0–114 kg, which indicates intensified interaction between lime and silica from the charge.

Within the broader temperature interval of 573–2073 K and at lime additions of 60–140 kg, the content of tricalcium silicate $3CaO{\cdot}SiO_2$ (Ca_3SiO_5) decreases from 156.42 to 7.72 kg. This behavior is associated with the redistribution of components in the slag system and the transfer of part of the calcium into CaO and Ca_2SiO_4, which are thermodynamically more stable at elevated temperatures.

As temperature and slag basicity increase, a sequential redistribution of calcium among different silicate compounds is observed. At moderate temperatures, calcium silicate phases predominate, indicating active binding of silica by lime. Further temperature increase leads to changes in phase composition and a higher fraction of more thermodynamically stable calcium-containing compounds.

The obtained dependencies reveal the mechanism of CaO interaction with charge silica and confirm the significant influence of lime consumption and temperature conditions on slag phase composition and physicochemical properties.

Figure 4 shows the dependence of manganese-containing compounds in the slag phase on temperature and lime consumption (CaO). The thermodynamic modeling results in the temperature range of 573–2073 K reflect the distribution of manganese among various oxide and silicate phases in the slag.

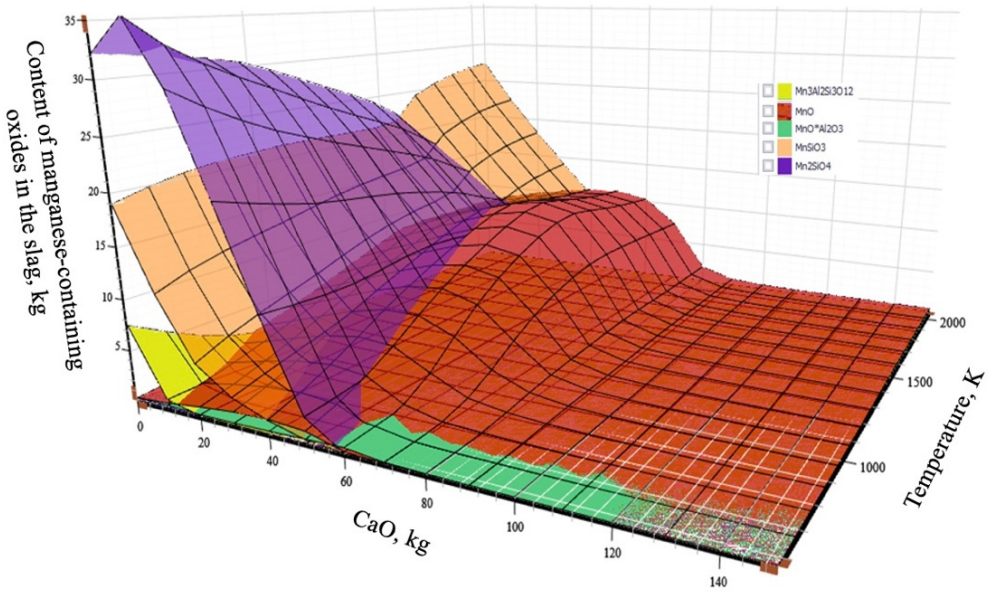


Figure 4. Dependence of the Content of Manganese-Containing Oxide Compounds in Slag on Temperature and Lime Consumption.

In the absence of lime, within the temperature range of 573–1073 K, up to 7.49 kg of spessartine ($Mn_3Al_2Si_3O_{12}$) is formed, which decomposes with further temperature increase to produce manganese oxide (MnO). At temperatures around 500 K and lime additions of 0–140 kg, manganese metasilicate $MnSiO_3$ is present in the slag in amounts ranging from 18.98 to 0.06 kg. With increasing temperature and lime consumption, up to 60 kg of manganese orthosilicate Mn_2SiO_4 is formed, which at higher temperatures also converts into manganese oxide.

A decrease in the content of manganese-containing oxide compounds at lime additions of 90–140 kg indicates intensification of reduction processes and the transfer of manganese into the metallic phase. This confirms that increasing slag basicity reduces manganese losses to the slag and improves conditions for its recovery into the metal.

At low lime additions and lower temperatures, the slag phase is dominated by complex manganese-containing oxide and silicate compounds, indicating a limited degree of manganese binding in stable calcium-containing phases. As the CaO content increases, the slag phase composition changes, accompanied by redistribution of manganese and a decrease in the fraction of individual manganese compounds due to the formation of more thermodynamically stable complex phases, such as dicalcium silicate (Ca_2SiO_4), calcium silicate ($CaSiO_3$), and manganese silicates.

An increase in temperature further intensifies the redistribution of manganese among slag compounds and alters their thermodynamic stability. Overall, the established relationships demonstrate the significant influence of slag basicity and temperature conditions on the phase state of manganese and the conditions of its retention in the slag phase.

Figures 5 and 6 show the dependence of manganese and silicon contents in the metallic phase on lime consumption in the charge. It was found that at lime additions of 70–140 kg and temperatures of 1273–2073 K, the manganese content in the metal reaches 81–83 wt.% (Figure 5).

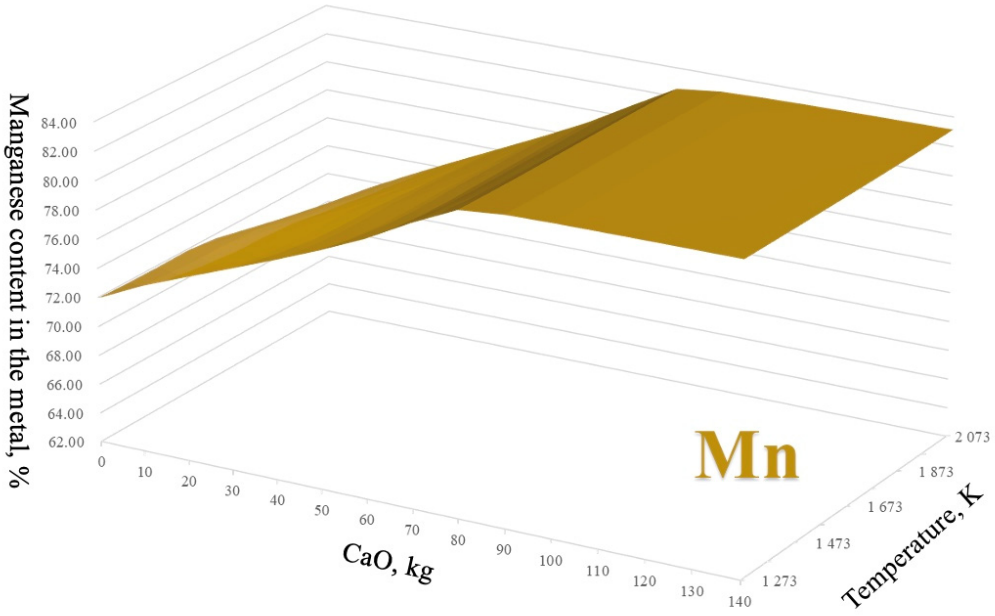


Figure 5. Dependence of Manganese Content in the Metallic Phase on Temperature and Lime Consumption.

Starting from a lime consumption of approximately 70 kg, a decrease in silicon content in the metallic phase is observed (Figure 6), indicating enhanced silicon binding in the slag and its transfer into silicate compounds. The obtained dependencies confirm the significant influence of slag basicity on the distribution of manganese and silicon between the metallic and slag phases.

Table 3 presents the calculated metal composition determined based on thermodynamic modeling of the process. According to the results of the comprehensive thermodynamic modeling of the medium-carbon ferromanganese smelting process, the optimal lime consumption was determined. It was established that at a lime addition of 90 kg and within the temperature range of 1673–1873 K, the manganese content in the metal is 82.95–82.93 wt.%, while the silicon content is 2.78–2.77 wt.%.

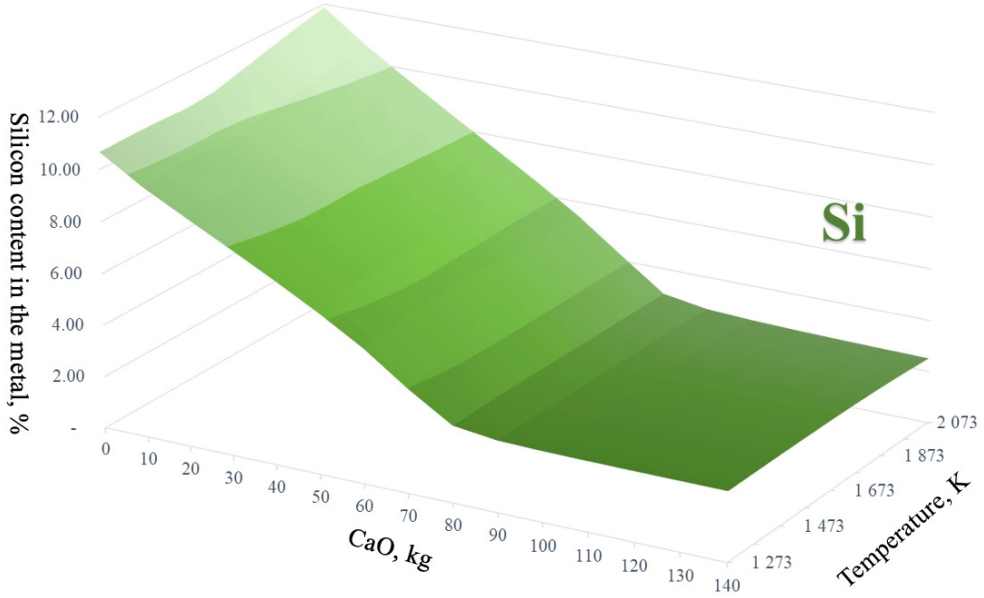


Figure 6. Dependence of Silicon Content in the Metallic Phase on Temperature and Lime Consumption.

Table 3. Metal Composition, wt.%.

T, K	Mn	Fe	Si	C
1473	82.97	12.56	2.77	1.70
1573	82.96	12.56	2.78	1.70
1673	82.95	12.57	2.78	1.70
1773	82.94	12.59	2.77	1.70
1873	82.93	12.60	2.77	1.70
1973	82.92	12.62	2.76	1.70
2073	82.91	12.64	2.74	1.71

The obtained manganese content values meet the requirements of the state standard (GOST 4755-91) [35] for medium-carbon ferromanganese; however, the silicon content exceeds the regulatory limit, as its concentration must be below 2.0%.

In this regard, further thermodynamic investigation should be carried out at a fixed lime consumption of 90 kg, followed by an analysis of the effect of varying manganese ore consumption on the composition of the metallic phase.

At high temperatures, the formation of a liquid slag phase was taken into account in the thermodynamic calculations. The liquid phase was considered an oxide melt under equilibrium conditions, and the distribution of elements between metal, slag, and gas phases was calculated accordingly. The graphical results are presented in terms of phase composition and do not explicitly distinguish between solid and liquid states.

3.1.2. Thermodynamic Modeling of Medium-Carbon Ferromanganese Smelting as a Function of Manganese Ore Consumption

For the comprehensive thermodynamic modeling, the consumption of manganese ore and lime per 100 kg of ferrosilicomanganese is presented in Table 4.

Table 4. Consumption of Charge Materials, kg.

FeSiMn 17	Manganese Ore	Lime
100	100–170/10	90

Ore consumption was varied in the range of 100–170 kg with a step of 10 kg. Figure 7 shows the dependence of calcium-containing oxide compounds in the slag phase on temperature and the amount of Mn_2O_3 in the system. The manganese content of the ore was represented in the form of Mn_2O_3, recalculated from the total manganese content ($Mn_{general}$) assuming complete oxidation to Mn_2O_3. The thermodynamic modeling results illustrate the distribution of calcium among different compounds, including free CaO and complex calcium silicates of various compositions.

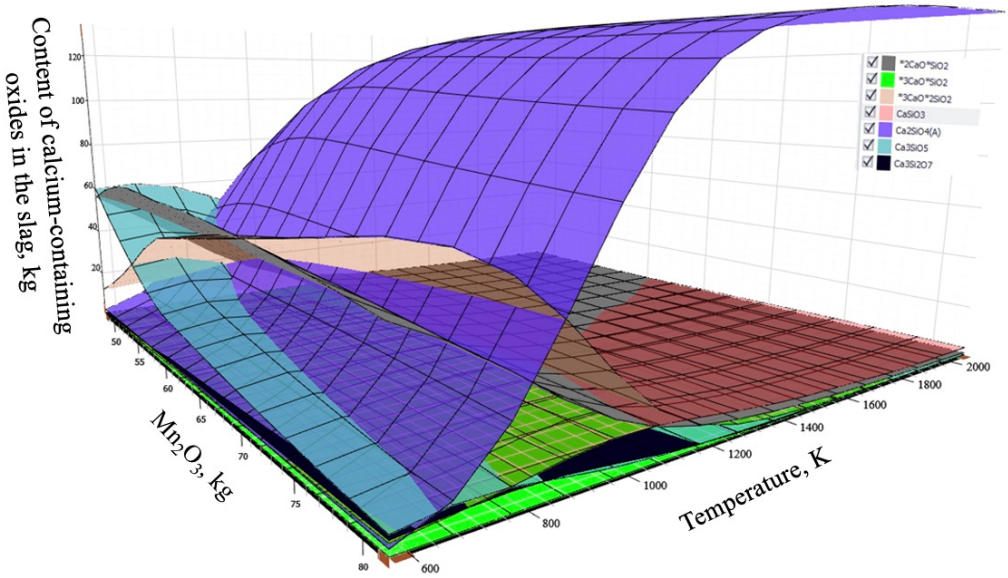


Figure 7. Dependence of the Content of Calcium-Containing Oxide Compounds in Slag on Temperature and Manganese Ore Consumption.

The influence of temperature and manganese ore consumption on the slag phase composition was investigated by thermodynamic modeling in the temperature range of 500–2000 K at manganese ore additions of 100–170 kg. It was established that within the temperature range of 573–1273 K, the slag phase is predominantly composed of calcium-containing silicate compounds, including $2CaO{\cdot}SiO_2$ (Ca_2SiO_4), $CaSiO_3$, Ca_3SiO_5, and $Ca_3Si_2O_7$.

At temperatures above 1273 K, the preferential formation of dicalcium silicate Ca_2SiO_4 is observed, indicating its higher thermodynamic stability in the high-temperature region.

At relatively low temperatures and elevated Mn_2O_3 content (i.e., increased manganese input from the ore, corresponding to approximately 55–80 kg Mn_2O_3 in the system), a significant portion of calcium is concentrated in silicate phases due to the active interaction of CaO with silica and components of the manganese-containing system.

In the high-temperature region, the fraction of thermodynamically more stable calcium-containing phases increases, while the content of intermediate compounds decreases. The obtained dependencies indicate a significant influence of manganese oxide content and temperature conditions on the slag phase composition and the mechanisms of calcium binding in the slag system.

Figure 8 shows the dependence of manganese-containing oxide compounds in the slag phase on temperature and the amount of Mn_2O_3 in the system. The thermodynamic

modeling results reflect the distribution of manganese among the main oxide and silicate phases in the slag.

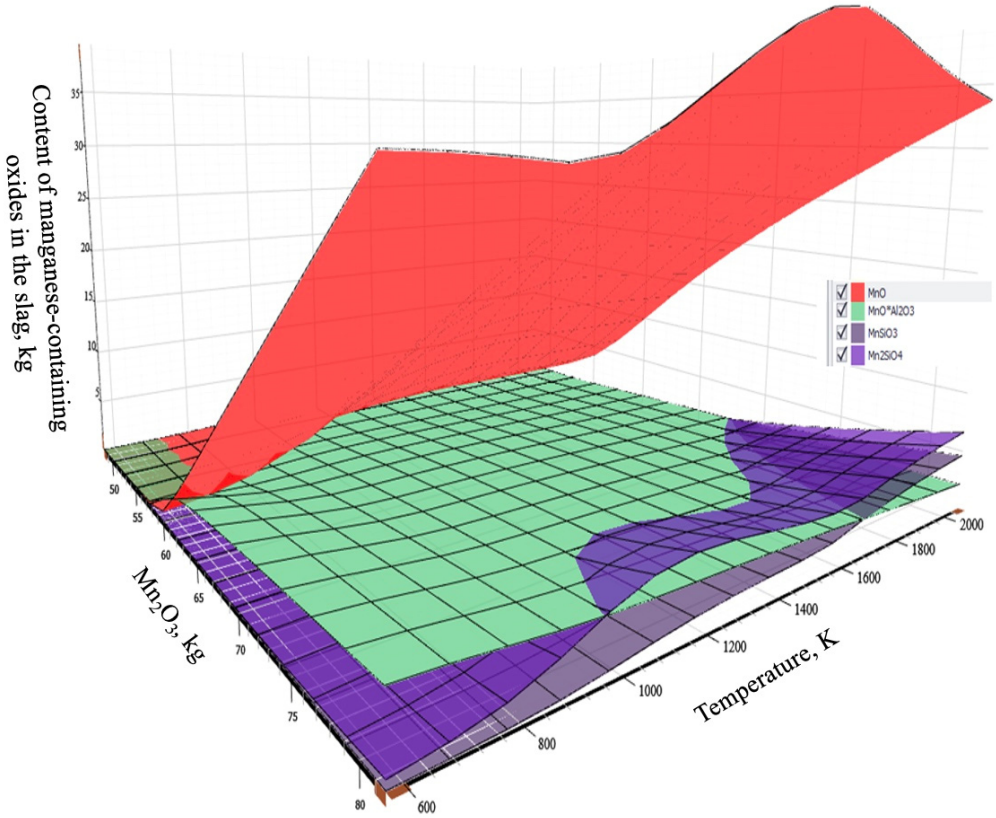


Figure 8. Dependence of the Content of Manganese-Containing Oxide Compounds in Slag on Temperature and Manganese Ore Consumption.

It was established that increasing manganese ore consumption intensifies the formation of manganese oxide (MnO), which becomes the predominant form of manganese in the slag at high temperatures.

At low ore additions (up to 50 kg) and within the temperature range of 573–2073 K, complex manganese compounds are mainly formed, including $MnO \cdot Al_2O_3$, $MnSiO_3$, and Mn_2SiO_4. In the low-temperature region, a significant portion of manganese is concentrated in silicate phases due to its binding with slag silica.

As temperature increases, the slag phase composition changes, accompanied by a progressive increase in the fraction of simple manganese oxide (MnO) in the slag and a simultaneous decrease in the content of complex manganese silicates. This behavior is associated with their thermal instability and decomposition into MnO, which represents a more stable intermediate oxide form at elevated temperatures.

The obtained dependencies indicate that temperature is the determining factor governing the phase state of manganese in the slag and significantly influences its distribution between slag and metal phases.

Figures 9 and 10 show the dependence of manganese and silicon contents in the metallic phase on manganese ore consumption.

It was found that at manganese ore additions of 100–170 kg and temperatures of 1273–2073 K, the manganese content in the metal ranges from 81 to 84 wt.% (Figure 9). The highest manganese contents, 83.80–83.92 wt.%, are achieved at an ore consumption of approximately 110 kg. Under these conditions, the silicon content in the metallic phase is 1.78–1.80 wt.% (Figure 10).

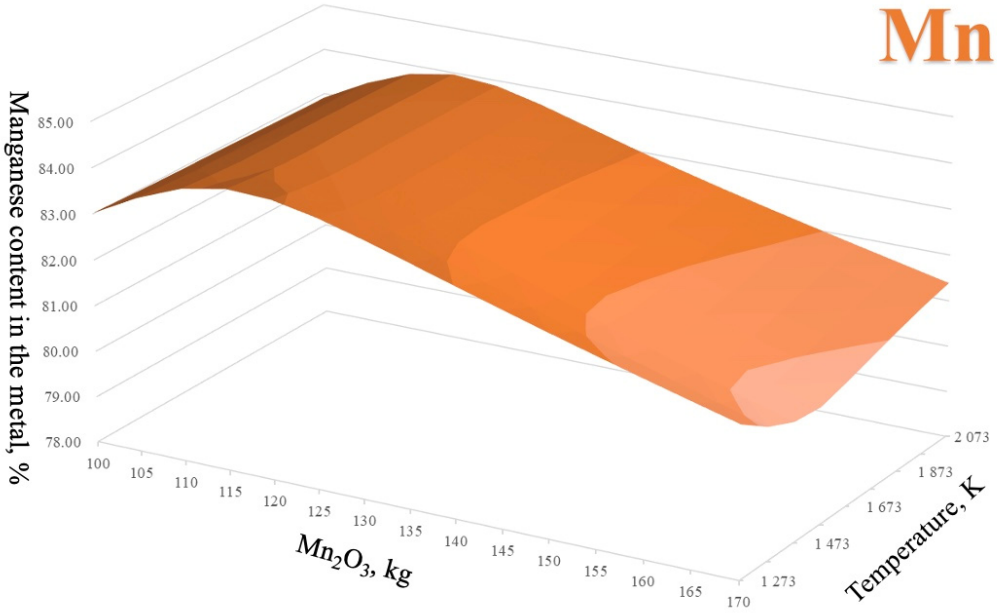


Figure 9. Dependence of Manganese Content in the Metallic Phase on Temperature and Manganese Ore Consumption.

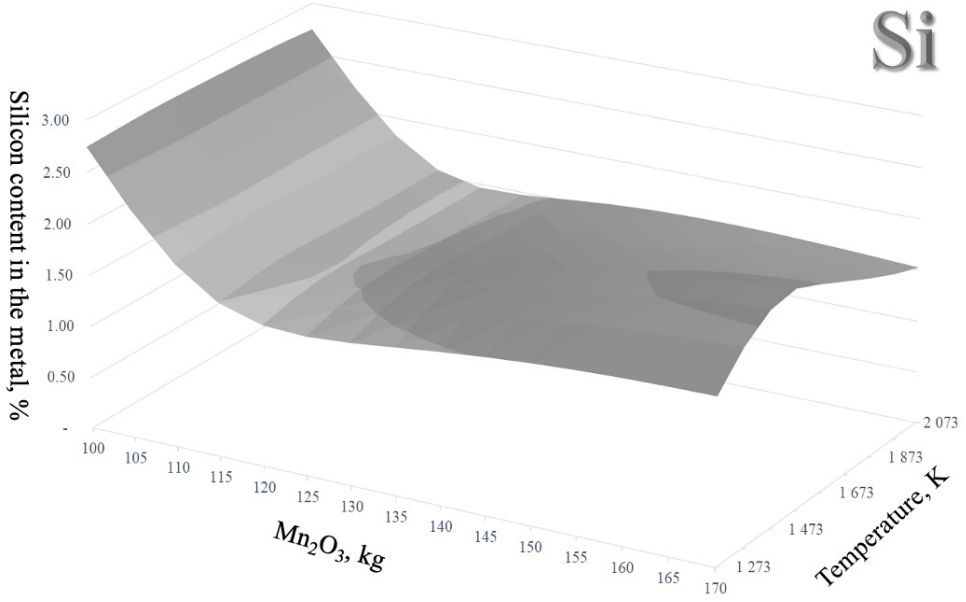


Figure 10. Dependence of Silicon Content in the Metallic Phase on Temperature and Manganese Ore Consumption.

Table 5 presents the calculated metal composition determined based on thermodynamic modeling of the process. According to the results of the comprehensive thermodynamic modeling of the medium-carbon ferromanganese smelting process, the optimal consumptions of lime and manganese ore were determined to be 90 and 110 kg, respectively. Within the temperature range of 1673–1873 K, the manganese content in the metallic phase exceeds approximately 83 wt.%, while the silicon content is below approximately 2.0 wt.%.

According to the results of the comprehensive thermodynamic modeling, the calculated chemical composition of the investigated metal is (wt.%): Mn 83–85; Si 1.8–2.0; Fe 12–13; C 1.5–1.7. This composition corresponds to commercially available medium-carbon ferromanganese and meets the requirements of relevant standards (e.g., GOST 4755-91) [35].

Table 5. Metal Composition, wt.%.

T, K	Mn	Fe	Si	C
1473	83.83	12.65	1.84	1.68
1573	83.83	12.65	1.84	1.68
1673	83.84	12.65	1.83	1.68
1773	83.84	12.66	1.83	1.68
1873	83.83	12.67	1.82	1.68
1973	83.82	12.68	1.82	1.68
2073	83.80	12.70	1.82	1.68

3.2. Experimental Smelting

3.2.1. Laboratory Smelting

Laboratory smelting experiments in the Tamman furnace were carried out in a corundum crucible, into which the charge materials—manganese ore, ferrosilicomanganese, and lime—were loaded. The composition of the charge mixture is presented in Table 6.

Table 6. Composition of the Charge Mixture.

Raw Materials, Versions (B-Basicity Slag)	Materials, g		
	Manganese Ore	FeSiMn 17	Lime
1.6	59	53	49
1.8	59	53	55

In all experimental melts, gas evolution was observed through the walls of the graphite (carbon) tube cover when the temperature reached approximately 930 °C. The onset of melting of the charge materials was noted at around 1200 °C. The formation of a liquid melt was detected at approximately 1400 °C and was monitored using a probe made of tungsten-molybdenum wire.

At 1600 °C, metallic and slag phases were fully formed in the crucible. At this temperature, the melt was held for 30–45 min, after which the furnace was cooled. When the temperature decreased to approximately 200 °C, the alumina crucible was removed from the furnace. The use of an alumina (Al_2O_3) crucible ensured chemical inertness and prevented additional carbon input into the system, which could otherwise affect the reduction process and metal composition. Figure 11 shows a cross-sectional view of the crucible with separated metallic and slag phases.

To determine the optimal conditions, the amount of FeSiMn was varied. During the laboratory experiments, the reduction process in the crucible proceeded intensively, accompanied by complete melting of the charge and clear separation of metal and slag.

The chemical compositions of the obtained metallic and slag phases were determined using classical chemical ("wet") analysis methods. The contents of manganese, iron, silicon, carbon, and phosphorus in the metal, as well as MnO, SiO_2, CaO, and MgO oxides in the slag, were determined using standard analytical procedures involving acid digestion of the samples followed by titrimetric and gravimetric determination of the components.



Figure 11. Appearance of the Metal and Slag.

The results of the chemical analysis are presented in the table. The obtained data indicate a high manganese content in the metallic phase (83.54–84.81 wt.%) with reduced silicon and phosphorus contents, which meets the requirements for medium-carbon ferromanganese. The slag phase is predominantly composed of calcium, silicon, and manganese oxides, reflecting the formation of a basic silicate slag during smelting.

The chemical composition of the slag, and especially its basicity (CaO/SiO_2 ratio), has a significant influence on several technological parameters of the process. As shown in Table 6, the slag basicity ranged from 1.6 to 1.8. The selected basicity level largely determines the technological properties of slag. The chemical composition of the metal and slag obtained from laboratory smelting is presented in Table 7.

Table 7. Chemical Composition of the Metal and Slag, wt.%.

Metal					Slag			
Mn	**Fe**	**Si**	**C**	**P**	**MnO**	**SiO_2**	**CaO**	**MgO**
83.54	11.36	2.13	0.95	0.161	17.90	21.45	36.92	7.94
84.81	10.4	0.6	1.46	0.137	11.79	22.19	36.92	10.83

In this case, the main objective was to improve the technical and economic performance of the process, including the recovery of the main element into the alloy, slag processability, and slag volume ratio. The manganese recovery from the ore into the alloy was ≥63%, which contributed to the formation of a stable slag not prone to self-disintegration.

The process was characterized by clear separation of metallic and slag phases. The slags obtained during the laboratory experimental smelting had a dense, stone-like structure and did not show signs of disintegration. The reported optimal performance indicators correspond to a slag basicity range of 1.6–1.8.

3.2.2. Large-Scale Laboratory Smelting

Charging of the burden materials was carried out continuously in a batchwise mode (the mass of a single batch charged into the furnace was 100 kg). Every two hours, tapping of the metal into cast iron molds was performed using a steel rod. Metal tapping from the furnace proceeded actively, with the mass of metal per tap ranging from 30 to 45 kg. The duration of a single smelting operation was 100–120 min. The current during smelting was maintained at 100–120 A.

The metal and slag were tapped from the furnace in an overheated state, and the slag exhibited high chemical reactivity. The appearance of the metal and slag tapping process is shown in Figure 12.



Figure 12. Alloy tapping.

The overall performance of the furnace was characterized by stable smelting operation, as confirmed by a steady current load and timely metal tapping. After each tap, the obtained metal and slag were weighed, and samples were taken for chemical analysis (Table 8).

Table 8. Chemical Composition of the Metal and Slag, wt.%.

No.	Metal						Slag				
	Mn	**Si**	**C**	**P**	**S**	**Fe**	**MnO**	**CaO**	**Al_2O_3**	**MgO**	**SiO_2**
1	87.98	0.02	1.7	0.06	0.05	10.05	15.75	40.85	8.81	10.65	21.05
2	88.15	0.04	1.5	0.04	0.03	9.99	15.65	40.75	8.84	10.65	20.95
3	88.65	0.03	1.7	0.07	0.04	10.01	14.95	40.71	8.45	10.56	20.94
4	88.11	0.03	1.5	0.03	0.02	9.89	14.50	40.68	8.35	10.53	20.90
5	87.79	0.03	1.6	0.05	0.05	9.89	14.35	40.75	8.15	10.51	20.89
Average	88.14	0.03	1.6	0.05	0.03	9.97	15.04	40.75	8.50	10.58	20.98

Based on the results of the large-scale laboratory experiments, the performance indicators for medium-carbon ferromanganese smelting in a furnace equipped with a 100 kVA transformer are presented in Table 9.

Table 9. Performance Indicators of Medium-Carbon Ferromanganese Smelting in a Furnace with a 100 kVA Transformer.

Material Consumption, kg	
Manganese ore	111
SiMn17	100
Lime	94
Metal	
Manganese recovery, %	65–70
Total metal weight, kg	150
Slag	
Slag basicity	1.8–1.9
Total slag weight, kg	205

Carbon in the thermodynamic calculations was considered as part of ferrosilicomanganese and as elemental carbon (C) in the system. However, additional carbon input from electrode consumption (~0.1 kg per heat) during large-scale smelting was not included in the model. This led to differences between the modeled and actual carbon balance.

Moreover, the calculations assume equilibrium conditions and do not account for kinetic limitations. Under real conditions, high slag basicity reduces the activity of SiO_2 and promotes its retention in the slag as calcium silicates, thereby limiting silicon reduction. These factors contribute to the discrepancy between calculated and experimental silicon contents.

The results of the large-scale laboratory smelting (Table 8) demonstrate a high manganese content in the metallic phase (≈88 wt.%), which is in good agreement with the thermodynamic predictions. However, a significant discrepancy is observed for silicon. According to thermodynamic modeling, the silicon content in the metal is expected to be approximately 1.8–2.0 wt.%, whereas in the experimental melts, it is extremely low (0.02–0.04 wt.%).

This pronounced deviation can be explained by the specific physicochemical conditions of the smelting process. Under industrial-like conditions, the reduction of SiO_2 is strongly limited by kinetic factors, including mass transfer resistance, slag viscosity, and insufficient interaction time between the carbon reductant and silica.

In addition, the formation of a highly basic CaO-SiO_2 slag (CaO ≈ 40 wt.%) promotes the stabilization of silicon in the form of calcium silicates, thereby suppressing its reduction and transfer into the metallic phase. The high basicity of the slag significantly decreases the activity of SiO_2, making its reduction thermodynamically less favorable under real conditions compared to ideal equilibrium assumptions.

Furthermore, part of the silicon may be re-oxidized during metal-slag interaction or remain dissolved in the slag phase due to incomplete reduction. These factors collectively result in substantially lower silicon content in the metal compared to calculated values.

Thus, the discrepancy between calculated and experimental silicon contents highlights the dominant role of slag chemistry and kinetic limitations in controlling silicon behavior during medium-carbon ferromanganese smelting.

3.3. Microstructural Analysis

To determine the phase composition, morphology, and elemental distribution in the obtained medium-carbon ferromanganese, microstructural investigations were carried out using scanning electron microscopy combined with energy-dispersive spectroscopy (SEM-EDS). This approach makes it possible not only to visualize the structural constituents of the alloy but also to determine their local chemical composition, which is especially important for multicomponent manganese ferroalloys formed under reducing smelting conditions.

The study was aimed at identifying the metallic matrix, secondary phases, and possible carbide or silicide inclusions, as well as evaluating the microstructural homogeneity of the obtained alloy.

The electron micrograph of medium-carbon ferromanganese (Figure 13) shows a pronounced heterogeneous microstructure characteristic of multicomponent ferroalloys in the Fe-Mn-Si-C system. The structure consists of a light metallic matrix, within which regions of varying morphology and contrast are distributed, reflecting differences in the chemical composition of the phases.

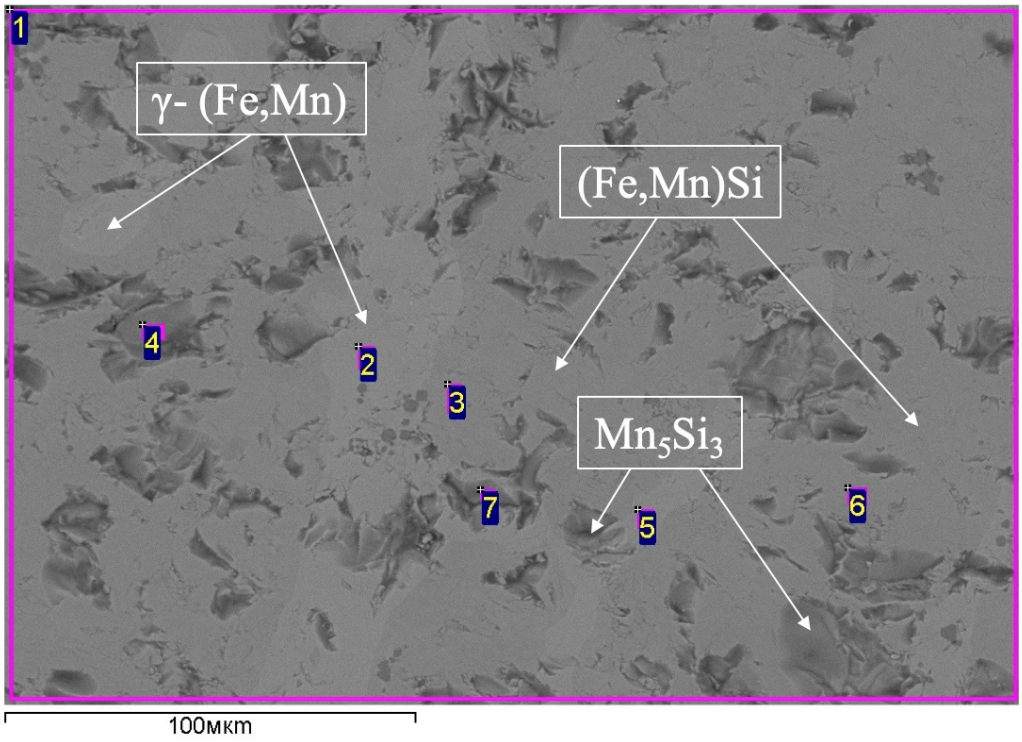


Figure 13. SEM Micrograph of the Alloy Microstructure.

The results of the quantitative EDS analysis performed on the selected microstructural areas (Spectra 1–7) are summarized in Table 10. The data reflect the elemental distribution in the examined regions and confirm the heterogeneity of the alloy structure, which is associated with phase differentiation during solidification.

Table 10. Quantitative EDS Analysis of Selected Areas (Spectra 1–7), mass.%.

Spectrum	Al	Si	Mn	Fe
1	-	21.3	68.7	10.0
2	-	16.2	70.2	13.7
3	-	23.6	66.7	9.7
4	1.1	19.5	67.6	11.8
5	-	15.9	70.9	13.2
6	-	23.7	68.0	8.2
7	1.5	5.7	72.7	20.1

In backscattered electron (BSE) mode, the SEM image clearly distinguishes regions with different average atomic numbers, appearing as bright and darker areas, which indicates the phase heterogeneity of the alloy. According to the results of local SEM-EDS analysis (spectra 1–7), the main elements in the investigated microzones are manganese and silicon, with variable iron content.

The bulk of the material is formed by a light-gray metallic matrix corresponding to the γ-solid solution of the (Fe,Mn) system, in which the manganese content reaches approximately 67–73 mass.% and iron up to about 20 mass.%. Within the matrix, darker regions enriched in silicon (up to ~23–24 mass.%) and characterized by lower iron content are observed. These areas correspond to silicon-containing intermetallic phases, silicides of the (Fe,Mn)Si and Mn_5Si_3 types.

The observed microstructure indicates a multiphase structure of the alloy and the formation of silicide phases during crystallization of the metallic melt upon cooling. The relatively uniform distribution of manganese in most analyzed points indicates a high degree of completion of the reduction processes during smelting. The absence of large isolated nonmetallic inclusions and sharp phase boundaries suggests stable thermodynamic conditions and satisfactory crystallization behavior.

The slag formed during medium-carbon ferromanganese smelting plays a key role in establishing the metallurgical conditions of the process. It functions as a thermodynamic and kinetic regulator of reduction reactions, influences the recovery of manganese and silicon into the metallic phase, and determines the distribution of impurities between metal and slag. In addition, the composition and structure of the slag significantly affect the thermal regime of smelting, melt viscosity, and the intensity of mass transfer in the "metal-slag-gas" system.

To determine the phase composition, morphology, and elemental distribution in the slag phase, investigations were carried out using scanning electron microscopy combined with energy-dispersive spectroscopy (SEM-EDS). This approach makes it possible to characterize in detail the structural heterogeneity of the slag and identify mineral phases formed under the reducing smelting conditions of manganese alloys. The results of the quantitative EDS analysis performed on the selected microstructural areas (Spectra 1–7) are summarized in Table 11.

Table 11. Quantitative EDS Analysis of Selected Areas (Spectra 1–7), mass.%.

Spectrum	O	Mg	Al	Si	Ca	Mn	Fe
1	45.4	2.2	15.5	4.4	19.4	12.5	0.1
2	45.0	-	-	15.2	38.2	1.5	0.0
3	32.3	10.2	2.3	1.7	3.7	49.6	0.2
4	46.7	-	17.9	4.0	22.4	9.0	0.1
5	32.9	11.0	-	0.8	4.6	50.4	0.4
6	44.1	-	-	15.6	39.3	1.0	0.0
7	37.1	9.6	-	1.2	5.0	46.7	0.3

The electron micrograph of the slag formed during medium-carbon ferromanganese smelting (Figure 14) reveals a pronounced crystalline structure with signs of directional crystallization. The slag exhibits a layered and cracked morphology, which is associated with thermal stresses during cooling and differences in the thermal expansion coefficients of individual phases.

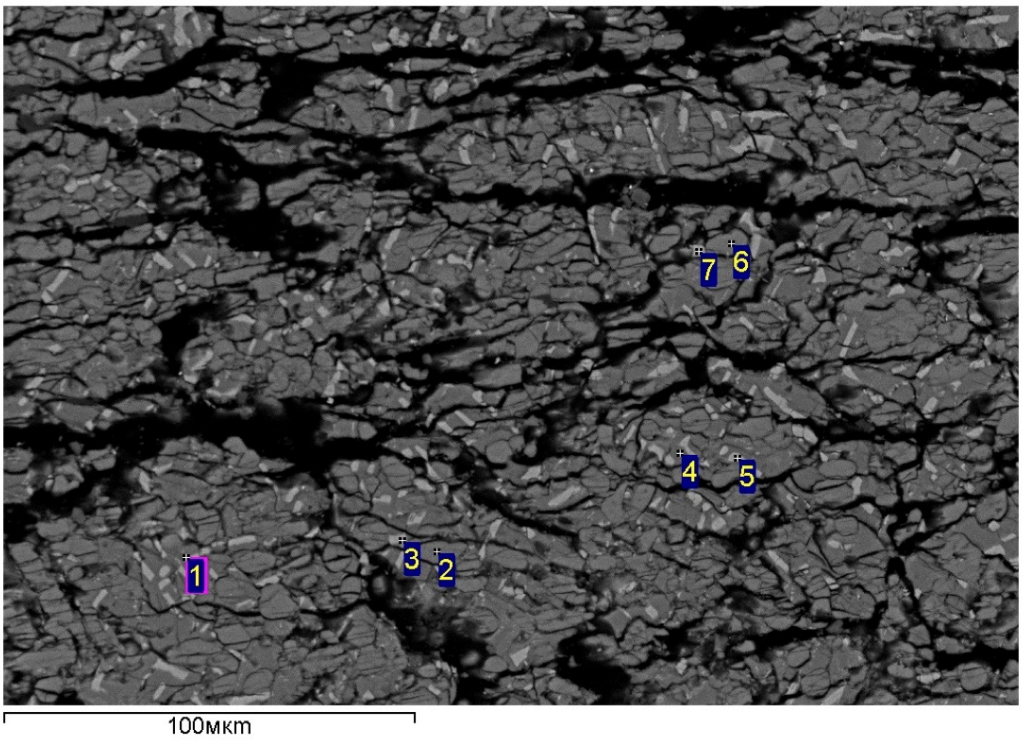


Figure 14. SEM Micrograph of the Slag Microstructure.

In backscattered electron (BSE) mode, phases with different average atomic numbers are clearly distinguished, indicating chemical and phase heterogeneity of the slag. The main volume of the structure is represented by a gray crystalline matrix, in which lighter and darker irregularly shaped regions are distributed.

According to the results of local EDS analysis (spectra 1–7), the slag has a complex oxide composition. The predominant components are oxygen, silicon, calcium, aluminum, and manganese, indicating the formation of a multicomponent silicate-aluminosilicate system.

Light regions (spectra enriched in Ca and Al) correspond to calcium aluminosilicate phases that form the crystalline framework of the slag. Darker areas enriched in silicon and

oxygen belong to the silicate glassy matrix. At several points, a noticeable manganese content in oxide form (up to ~39 mass.%) is detected, indicating partial retention of manganese in the slag phase and incomplete reduction into the metal.

The presence of areas containing trace amounts of iron indicates the involvement of impurity components from the raw materials in the slag phase and their redistribution during smelting.

The morphology of the crystalline phases—elongated and equiaxed grains oriented along cooling directions—indicates crystallization of the slag from the melt during temperature decrease. The cracked structure is caused by the shrinkage phenomena and vitrification of part of the silicate phase.

The investigated slag represents a heterogeneous oxide system of the silicate-aluminosilicate type with dissolved manganese and calcium oxides. Its phase composition and microstructure confirm active interaction between the slag and the reducing environment and reflect the thermodynamic conditions of medium-carbon ferromanganese smelting.

A comparison of bulk chemical analysis of the metal, slag composition data, and local SEM-EDS analysis provides a comprehensive understanding of the phase and chemical structure of the obtained medium-carbon ferromanganese.

According to laboratory smelting results (Table 7), the metal contains 83.5–84.8 wt.% Mn and 0.6–2.1 wt.% Si. At the same time, the slag contains significant amounts of MnO (11.8–17.9 wt.%) and SiO_2 (21.5–22.2 wt.%), indicating partial oxidation of manganese and silicon and incomplete reduction under laboratory furnace conditions.

During large-scale laboratory smelting (Table 8), a higher degree of manganese reduction was observed: the Mn content in the metal increased on average to 88.1 wt.%, while the silicon concentration decreased to ~0.03 wt.%. At the same time, the MnO content in the slag decreased (to an average of 15.0 wt.%) while maintaining a high CaO level (~40.7 wt.%), indicating a more basic slag and more efficient reduction processes. The decrease in silicon content in the metal is associated with its preferential transfer into the slag phase as SiO_2 (≈21 wt.%) at higher slag basicity; under commercially relevant conditions for medium-carbon ferromanganese, the maximum expected Si content in the metal is typically $\leq$ ~2.0 wt.%, which agrees with our thermodynamic estimates for the optimal charge.

Local quantitative EDS analysis of the metal from large-scale laboratory smelting (Table 10) shows that in individual microzones, the silicon content reaches 15–24 mass.%, with a simultaneously elevated manganese content (66–71 mass.%). These regions correspond to secondary silicide or silicomanganese phases. At the same time, in most analyzed points, the metallic matrix is enriched in manganese (up to 72.7 mass.%) and iron (up to 20.1 mass.%), with reduced silicon content (5–6 mass.% and lower).

Thus, the difference between the bulk chemical composition of the metal (Si ≈ 0.03–2.1 wt.%) and the local SEM-EDS data (Si up to 24 mass.% in individual points) is explained by the microphase heterogeneity of the alloy. Energy-dispersive spectroscopy records the composition of individual microphases, whereas chemical analysis reflects the averaged composition of the entire metal volume. The small volumetric fraction of silicon-containing phases leads to their high local composition, having little effect on the overall silicon content in the alloy.

The obtained data confirm that the microstructure of medium-carbon ferromanganese after large-scale laboratory smelting is represented by a manganese-iron metallic matrix with finely dispersed silicide microphases. Such a structure is a characteristic structural feature of reduction-produced manganese ferroalloys.

The results of microstructural studies and local chemical analysis of the slag are in good agreement with thermodynamic modeling data on the distribution of elements between metal and slag phases. Calculations showed that under the selected temperature and reducing conditions, part of the manganese and silicon remains in oxide form, participating in the formation of silicate and complex oxide compounds. This is confirmed by EDS data revealing the presence of manganese in slag phases.

The predominance of a silicate matrix in combination with calcium- and aluminum-containing compounds indicates the formation of a slag with a developed crystalline structure and reduced chemical activity with respect to the metallic phase at the final stages of smelting. Such a composition contributes to stabilization of the slag melt, reduction of its oxidizing capacity, and limitation of secondary oxidation of reduced metals.

The observed heterogeneity in manganese distribution within the slag reflects kinetic features of reduction processes and subsequent melt crystallization. Part of the manganese oxides does not have sufficient time to be completely reduced and becomes fixed in the silicate structure of the slag, which corresponds to the calculated equilibrium distribution of components in the "metal-slag" system.

Thus, the combination of microstructural data and thermodynamic modeling results shows that slag formation during medium-carbon ferromanganese smelting is governed by complex interactions between the silicate matrix and manganese and calcium oxides, and its composition directly affects metal recovery and the efficiency of reduction processes.

4. Conclusions

Thermodynamic modeling of the smelting process of medium-carbon ferromanganese in the "manganese ore-ferrosilicomanganese-lime" system demonstrated the decisive influence of slag basicity and temperature on the distribution of Mn and Si between the metallic and slag phases. Under the calculated conditions, the optimal lime and ore consumptions ensured Mn > 83 wt.% and Si < 2 wt.% in the metal, which meets the requirements of GOST 4755-91.

Experimental smelting in a Tammann furnace at a temperature of 1600 °C confirmed the feasibility of producing medium-carbon ferromanganese from the studied raw materials and the formation of a basic silicate slag. Under laboratory conditions, metal containing 83.5–84.8 wt.% Mn and 0.6–2.1 wt.% Si was obtained, while the slag contained 11.8–17.9 wt.% MnO, indicating partial retention of manganese in the oxide phase.

Large-scale laboratory experiments in a 100 kVA electric arc furnace were characterized by stable process operation (steady current load and regular metal tapping) and resulted in a higher degree of manganese reduction. The average metal composition was Mn 88.14 wt.%, Si 0.03 wt.%, C 1.6 wt.%, and Fe 9.97 wt.%, while the slag composition was MnO 15.04 wt.%, CaO 40.75 wt.%, and SiO_2 20.98 wt.% at a basicity of 1.8–1.9. Manganese recovery into the metal reached 65–70%.

It was established that increasing slag basicity leads to a decrease in silicon content in the metal due to its binding in the slag phase ($SiO_2 \approx 21$ wt.%) and simultaneously contributes to reduced manganese losses to the slag, which is a key factor in improving the technological performance of the process.

SEM-EDS analysis of the metal revealed a multiphase microstructure consisting of an Fe-Mn metallic matrix with finely dispersed silicide microphases. Local Si concentrations (up to 15–24 mass.% in individual microzones) explain the discrepancy with bulk chemical analysis and confirm the microphase heterogeneity of the alloy.

Microstructural and local chemical data for the slag showed the predominance of a silicate–aluminosilicate matrix involving Ca- and Al-containing phases, as well as the

presence of manganese in oxide form. This agrees with thermodynamic predictions of the inevitable retention of part of the manganese in the slag phase under the selected conditions.

Overall, the results confirm that coordinated control of slag basicity and composition is a decisive tool for increasing manganese recovery and stabilizing the process of medium-carbon ferromanganese production from Kazakhstan manganese raw materials. The obtained experimental and modeling data can serve as a basis for further optimization of operating parameters and technology scale-up.

Author Contributions: Conceptualization, A.A. and B.S.; methodology, A.A. and R.U.; software, R.U.; validation, A.A., B.S. and M.T.; formal analysis, A.A. and A.N.; investigation, A.A., B.S. and M.T.; resources, B.U.; data curation, M.T. and A.N.; writing—original draft preparation, A.A. and B.S.; writing—review and editing, B.U. and R.U.; visualization, A.N.; supervision, B.U.; project administration, B.U.; funding acquisition, B.U. All authors have read and agreed to the published version of the manuscript.

Funding: This research was funded by the Science Committee of the Ministry of Education and Science of the Republic of Kazakhstan (Grant No. AP23488066).

Data Availability Statement: The original contributions presented in this study are included in the article. Further inquiries can be directed to the corresponding authors.

Conflicts of Interest: The authors declare no conflicts of interest. The funders had no role in the design of the study; in the collection, analyses, or interpretation of data; in the writing of the manuscript; or in the decision to publish the results.

References

1. Sjöqvist, T.; Jönsson, P.; Grong, Ö. Inclusions in commercial low and medium carbon ferromanganese. *Metall. Mater. Trans. A* **2001**, *32*, 1049–1056. [CrossRef]
2. Tangstad, M. Manganese ferroalloys technology. In *Handbook of Ferroalloys*; Butterworth-Heinemann: Oxford, UK, 2013; pp. 221–266.
3. Coetsee, T. MnO reduction in high carbon ferromanganese production: Practice and theory. *Miner. Process. Extr. Metall. Rev.* **2018**, *39*, 351–358. [CrossRef]
4. Eissa, M.; Ghali, S.; Ahmed, A.; El-Faramawy, H. Optimum condition for smelting high carbon ferromanganese. *Ironmak. Steelmak.* **2012**, *39*, 419–430. [CrossRef]
5. Kim, E.J.; You, B.D.; Pak, J.J. Thermodynamics of carbon in liquid manganese and ferromanganese alloys. *Metall. Mater. Trans. B* **2003**, *34*, 51–59. [CrossRef]
6. Ding, W.; Xu, W.; Tang, K.; Jiang, G. Optimization of Medium- and Low-Carbon Ferromanganese Process by Silicothermic Reduction. In Proceedings of the 8th International Ferroalloys Congress (INFACON 8), Beijing, China, 7–10 June 1998.
7. Olsen, S.E.; Tangstad, M.; Lindstad, T. *Production of Manganese Ferroalloys*; Tapir Academic Press: Trondheim, Norway, 2007.
8. Gasik, M.I. *Handbook of Ferroalloys: Theory and Technology*; Elsevier: Oxford, UK, 2013.
9. Tangstad, M.; Olsen, S.E. The Production of Refined Ferromanganese Alloys. In Proceedings of the INFACON 9, Quebec City, QC, Canada, 3–7 June 2001; pp. 617–626.
10. Supriyatna, Y.I.; Zulhan, Z.; Triapriani, Y. The ferromanganese production using Indonesian low-grade manganese ore using charcoal and palm kernel shell as reductant in mini electric arc furnace. *IOP Conf. Ser. Mater. Sci. Eng.* **2018**, *285*, 012022. [CrossRef]
11. Abdel Halim, K.S.; Bahgat, M.; Morsi, M.B.; El-Barawy, K. Pre-reduction of manganese ores for ferromanganese industry. *Ironmak. Steelmak.* **2011**, *38*, 279–284. [CrossRef]
12. Makhambetov, Y.; Zhakan, A.; Zhunusov, A.; Kabylkanov, S.; Burumbayev, A.; Sadyk, Z.; Akhmetov, A.; Uakhitova, B. Resource-Efficient Smelting Technology for FeCrMnSi Ferroalloy Production from Technogenic Wastes in an Ore-Thermal Furnace. *Metals* **2025**, *15*, 1318. [CrossRef]
13. Makhambetov, Y.; Abdulina, S.; Kabylkanov, S.; Burumbayev, A.; Zhakan, A.; Sadyk, Z.; Akhmetov, A. Production of Chromium–Manganese Ligature from Low-Grade Chromium and Iron–Manganese Ores Using Silicon–Aluminum Alloys as Reductants. *Processes* **2025**, *13*, 3158. [CrossRef]

14. Kosdauletov, N.; Suleimen, B.; Adilov, G.; Nurumgaliyev, A.; Kelamanov, B.; Kuatbay, Y.; Zhunuskaliyev, T.; Bulekova, G.; Salikhov, S.; Abdirashit, A. Thermodynamic and Experimental Analysis of the Selective Reduction of Iron by Hydrogen from the Kergetas Iron–Manganese Ore. *Metals* **2025**, *15*, 1330. [CrossRef]
15. IMnI ANNUAL REVIEW. Available online: https://www.manganese.org/sites/default/files/featured_images/2021-Annual-Review-EN.pdf (accessed on 30 October 2025).
16. U.S. Geological Survey. *Mineral Commodity Summaries 2024: Manganese*; USGS: Reston, VA, USA, 2024. Available online: https://pubs.usgs.gov/periodicals/mcs2024/mcs2024-manganese.pdf (accessed on 7 November 2025).
17. International Manganese Institute (IMnI). *Manganese Ore and Alloy Production Statistics*; IMnI: Paris, France, 2023; Available online: https://www.manganese.org (accessed on 8 November 2025).
18. Baisanov, S.O.; Abishev, D.N.; Serikbayev, B.A.; Kim, A.S. Thermodynamic and Technological Aspects of Processing Low-Grade Manganese Ores. *Metallurgist* **2015**, *59*, 123–130.
19. Sariev, O.R.; Dossenkenov, M.S.; Kelamanov, B.S.; Abdirashit, A.M. High-carbon ferromanganese smelting on high-base slags. *Kompleks. Ispolz. Miner. Syra* **2020**, *4*, 63–73. [CrossRef]
20. Sarkar, A.; Schanche, T.L.; Safarian, J. Isothermal Pre-Reduction Behavior of Nchwaning Manganese Ore in H_2 Atmosphere. *Mater. Proc.* **2023**, *15*, 58.
21. Tolymbekov, M.Z. Manganese ore industry of Kazakhstan. *Gorn. Zh.* **2007**, *2*, 2–5. (In Russian)
22. Samuratov, E.K.; Baisanov, A.S.; Tolymbekov, M.Z.; Makashev, A.S.; Mukhtarova, G.M. Integrated processing of iron–manganese ores of Central Kazakhstan. In Proceedings of the International Scientific Conference "Innovative Development and the Demand for Science in Modern Kazakhstan", Almaty, Kazakhstan, 11–12 November 2008; Part 2, pp. 161–166. (In Russian)
23. Buketov, E.A.; Gabdullin, T.G.; Takenov, T.D. *Metallurgical Processing of Manganese Ores in Central Kazakhstan*; Nauka: Almaty, Kazakhstan, 1979; 184p. (In Russian)
24. Baisanov, A.S. *Phase Equilibria and Kinetics of Pyrometallurgical Processing of Iron–Manganese Ores*; Zh. Abishev Chemical-Metallurgical Institute: Karaganda, Kazakhstan, 2007; 22p. (In Russian)
25. Gabdullin, T.G. *Physicochemical Generalization, Development, and Implementation of Low-Waste, Energy-Saving Technological Schemes and Processes for the Metallurgical Processing of Manganese Ores from Kazakhstan Deposits*; I.P. Bardin Research Institute of Ferrous Metallurgy: Moscow, Russia, 1992; 46p. (In Russian)
26. Esengaliyev, D.A. Development of Technology for Smelting Refined Ferromanganese Using Highly Basic Manganese Ores and Special Complex Alloys. Ph.D. Thesis, Abylkas Saginov Karaganda Technical University, Karaganda, Kazakhstan, 2020; 111p. (In Russian)
27. Makhambetov, Y.; Gabdullin, S.; Zhakan, A.; Saulebek, Z.; Akhmetov, A.; Zulhan, Z.; Mukanov, S. Production of Complex Fe-Si-Mn-Cr Ferroalloy Using High-Ash Coal: A Sustainable Metallurgical Approach. *Mater. Res. Express* **2024**, *11*, 056523. [CrossRef]
28. Makhambetov, Y.N.; Abdirashit, A.M.; Myngzhassar, Y.A.; Burumbayev, A.G.; Zhakan, A.M.; Onuralp, Y. Research on the Possibility of Obtaining Medium-Carbon Ferromanganese from the Djezdinskoe Deposit. *Kompleks. Ispolz. Miner. Syra (Complex Use Miner. Resour.)* **2024**, *331*, 101–108. [CrossRef]
29. Abdirashit, A.; Yessengaliyev, D.; Kelamanov, B.; Sariyev, O.; Abikenova, G.; Nurgali, N.; Almagambetov, M.; Zhuniskaliyev, T.; Kuatbay, Y.; Abylay, Z. Investigation of the Possibility of Obtaining Nickel-Containing Ferroalloys from Lateritic Nickel Ores by a Metallothermic Method. *Metals* **2025**, *15*, 428. [CrossRef]
30. Yessengaliyev, D.; Kelamanov, B.; Zayakin, O. Thermodynamic modeling of the recovery process of manganese by metallothermic method. *J. Chem. Technol. Metall.* **2022**, *57*, 1230–1234.
31. Makhambetov, Y.; Zhakan, A.; Gabdullin, S.; Akhmetov, A.; Burumbayev, A.; Zhunusov, A. Study on the synthesis of FeCrMnSi ferroalloy using technogenic raw materials. *Acta Metall. Slovaca* **2025**, *31*, 113–118. [CrossRef]
32. Kelamanov, B.; Yessengaliyev, D.; Sariev, O.; Akuov, A.; Samuratov, Y.; Zhuniskaliyev, T.; Kuatbay, Y.; Mukhambetgaliyev, Y.; Kolesnikova, O.; Zhumatova, A.; et al. Technological Analysis of the Production of Nickel-Containing Composite Materials. *J. Compos. Sci.* **2024**, *8*, 179. [CrossRef]
33. Kelamanov, B.; Abilberikova, A.; Abdirashit, A.; Sariyev, O.; Yessengaliyev, D.; Zhuniskaliyev, T.; Kuatbay, Y.; Uakhitova, B.; Nurzhanov, A. Carbothermic Reduction of Low-Grade Nickel Ores from the "Batamsha" Deposit: Modeling, Pilot-Scale Smelting, and Phase Analysis. *Processes* **2025**, *13*, 2107. [CrossRef]

34. Makhambetov, Y.; Sadyk, Z.; Zhakan, A.; Burumbayev, A.; Kabylkanov, S.; Myrzagaliyev, A.; Aubakirov, D.; Lu, N.; Akhmetov, A. Electric Arc Metallothermic Smelting of FeCr Using FeAlSiCa as a Reductant. *Materials* **2025**, *18*, 4221. [CrossRef] [PubMed]
35. *GOST 4755-91*; Ferromanganese. Specifications. Interstate Council for Standardization, Metrology and Certification: Moscow, Russia, 1991.

Disclaimer/Publisher's Note: The statements, opinions and data contained in all publications are solely those of the individual author(s) and contributor(s) and not of MDPI and/or the editor(s). MDPI and/or the editor(s) disclaim responsibility for any injury to people or property resulting from any ideas, methods, instructions or products referred to in the content.